JOURNAL OF SPACECRAFT AND ROCKETS
Vol. 42, No. 6, November–December 2005

Zero- and One-*g* Comparison of Surface Profile in Single-Curved Parabolic Membrane

Christopher G. Meyer* and Jack Leifer†
University of Kentucky, Paducah, Kentucky 42002-7380
Bernardo C. Lopez‡
Jet Propulsion Laboratory, California Institute of Technology, Pasadena, California 91109
and
David C. Jones§ and Boyd C. Caddell¶
University of Kentucky, Paducah, Kentucky 42002-7380

This experiment was designed to quantify the effects of gravity and boundary support conditions on a scale model of an orbiting, singly curved parabolic thin-film membrane antenna. A 1-m-scale model of the parabolic antenna and support system was constructed and tested on NASA's KC-135A Weightless Wonder microgravity aircraft. A fabric-backed membrane (76.2-μm Nylon, 12.7-μm Mylar, 12.7-μm adhesive, 0.1-μm Al) was placed in the test fixture designed for this work and tensioned using edge clamps that maintained the desired parabolic profile at the membrane boundaries. Targets for tracking the full-field surface deflection were provided by about 7000 3-mm dots stenciled on to the membrane surface. The membrane surface configuration was monitored by four digital cameras mounted in the test enclosure. Using photogrammetry, the high-resolution digital images taken in-flight (at 0-*g* conditions) and on the ground (at 1-*g*) were processed, and the three-dimensional location of each target visible in at least three images was calculated. It was found that under the same support conditions both structural wrinkling and sag in microgravity were significantly less pronounced than at 1-*g*.

Nomenclature

E	=	Young's modulus
g	=	acceleration of gravity
p	=	focal length
p_A	=	focal length of full-scale antenna
p_t	=	focal length of test article
t	=	membrane thickness
x	=	coordinate direction along linear projected span of a parabola, aligned with the tangent to the parabola's vertex
x_A	=	linear projected span of parabolic antenna (full-scale), aligned tangent to the parabola's vertex
x_t	=	linear projected span of parabolic test article, aligned tangent to the parabola's vertex
x'	=	coordinate direction along linear projected span of a parabola, passing through its endpoints
y	=	coordinate direction along height of parabolic curve (perpendicular to x)
y'	=	parabola coordinate (perpendicular to x')
z	=	cylindrical coordinate direction (perpendicular to plane of parabolic curvature)
z_A	=	cylindrical length of full-scale parabolic antenna
z_t	=	cylindrical length of test article
$\varepsilon_z(x')$	=	cylindrical component of applied membrane strain
$\sigma_z(x')$	=	cylindrical component of membrane stress
σ_1	=	first principal stress component
σ_2	=	second principal stress component

I. Introduction

THIS experiment was designed to quantify the effects of gravity and boundary support conditions on a scale model of an orbiting precipitation radar antenna.[1,2] This thin-film structure, under development for deployment by the end of this decade, will use a singly curved parabolic profile conforming to

$$y = x^2/4p \tag{1}$$

where the focal length $p_A = 1.89$ m, linear projected span $x_A = 5.3$ m measured from the apex, and cylindrical length $z_A = 5.3$ m (Fig. 1). The structure will be deployed and maintained in its final shape on orbit by an integrated support system designed to contact the antenna only at its edges. As currently envisioned, the antenna will orbit at altitudes ranging between 400 and 750 km, and it will operate at simultaneous scanning frequencies of 14 and 35 GHz.

To achieve a low areal mass density, the parabolic reflector will be fabricated from 25.4-μm (1-mil) metallized polyimide film. Its rms surface accuracy must be held below 0.17 mm over $\frac{1}{3}$ of the reflector area and 0.25 mm elsewhere, to maintain its desired beam characteristics.[1,2] However, it is well known that membrane elements supported in tension are prone to out-of-plane structural wrinkling, which here refers to the fully reversible, or elastic, out-of-plane deformations of a membrane (for which the term *rippling*[3] has also been used). This is in contrast to the term *material wrinkling*, which refers to irreversible (plastic) out-of-plane deformations that

Presented as Paper 2004-1736 at the AIAA/ASME/ASCE/AHS/ASC 45th Structures, Structural Dynamics, and Materials Conference, 12th AIAA/ASME/AHS Adaptive Structures Conference, 6th AIAA Non-Deterministic Approaches Forum, and 5th AIAA Gossamer Spacecraft Forum, Palm Springs, CA, 19–22 April 2004; received 16 May 2004; revision received 3 January 2005; accepted for publication 26 January 2005.

*Undergraduate Assistant; currently Engineer, PEBCO, 225 N 4th Street, Paducah, KY 42001. Member AIAA.

†Assistant Professor, Department of Mechanical Engineering; currently Assistant Professor, Trinity University, One Trinity Place, San Antonio, TX 78212. Member AIAA.

‡Mechanical Systems Engineer, MS 299-100, Research Division, 4800 Oak Grove Drive. Member AIAA.

§Undergraduate Assistant, P.O. Box 7380, Extended Campus Programs, Department of Mechanical Engineering. Student Member AIAA.

¶Undergraduate Assistant, Department of Mechanical Engineering; currently Engineer, Belcan, Inc., Lexington, KY 40507.

are permanently set into the membrane when its elastic limit has been exceeded. The amplitude of reversible structural wrinkles can exceed the rms surface accuracy requirement just specified by more than two orders of magnitude.[2–10]

The structural wrinkle configuration developed over the surface of a Gossamer membrane can vary dramatically, depending on the location of the supports and loading configuration, as well as membrane shape, thickness, and material parameters. In one experiment, a uniform tensile load was applied to a vertically mounted rectangular polyester membrane by clamping two opposite edges and then uniformly moving the top edge up. This membrane responded by producing structural wrinkles that possessed crests and troughs running along the direction of the applied displacement load (Fig. 2).[10] Similar results were produced by Jenkins et al. for an edge-loaded, 0.2286×0.1564 m$^2 \times 20e$–6 m thick Mylar (a registered trademark of the DuPont Corp., Wilmington, Delaware) membrane tested horizontally.[7]

Other support configurations, such as the corner tensioned square membranes studied by Blandino et al.,[4] cause more complex wrinkle patterns to develop. Regardless of the complexity of the wrinkle pattern, however, it has been shown that structural wrinkles are caused by localized buckling in the membrane, which occurs wherever σ_2, the second principal stress, becomes slightly negative. Hence the wrinkle crests and troughs that appear on the membrane surface indicate the local orientation of σ_1, the first principal stress, in the material.[5,6]

One effect on Gossamer membranes that has heretofore not been fully verified experimentally is the role that gravity plays in both structural wrinkle configuration and overall surface profile. Extensive ground testing of scale-model Gossamer structures in 1-g has been performed in both vacuum and air; Black and Leifer et al. observed both membrane sag and structural wrinkling for 1.0-m^2, 25-μm-thick aluminized polyimide membranes mounted horizontally under both edge and corner support.[9]

Although Gossamer structures are being designed, built, and tested in 1-g environments, they are intended to operate on orbit in 0-g environments, where both their static and dynamic responses can be quite different from those observed on Earth prior to launch. However, there are few options available for performing experimental tests on scaled membranes in a 0-g environment. Although 0-g testing of scale-model structures can be performed onboard the Space Station, numerous factors render that option prohibitive in most cases. An alternative is to place the experimental apparatus in a free-falling reference frame, which simulates a 0-g environment. Performing the same experiment under both 1-g and microgravity conditions allows the effects of gravity on a Gossamer system to be directly observed and evaluated. Such comparative experimental data are vital for the verification of numerical codes designed to predict both the static and dynamic behavior of full-scale Gossamer structures in operational (0-g) environments.

A free-falling experimental environment is available aboard NASA's KC-135A microgravity airplane, also known as the Weightless Wonder. (Note that the NASA KC-135 described herein has been replaced by a DC-9, scheduled to become fully operational in early 2005.) Flying in a parabolic trajectory, the aircraft is placed into a controlled free fall near its peak altitude that provides about 25 s of microgravity relative to its fuselage (Fig. 3). These periods of microgravity are interspersed with 40-s periods of 1.8-g conditions that take place near the bottom of its trajectory, as the KC-135A pulls out of its free fall. Used both for astronaut training and scientific experiments, each flight of the KC-135A provides about 30 short periods of near-zero gravity (Fig. 4). Other, ground-based options for simulating 0-g involve experimental platforms incorporated into drop towers; however, even the tallest of these, such as the 145-m high facility at the NASA Glenn Research Center, can provide only a maximum of 5.2 s of microgravity conditions.

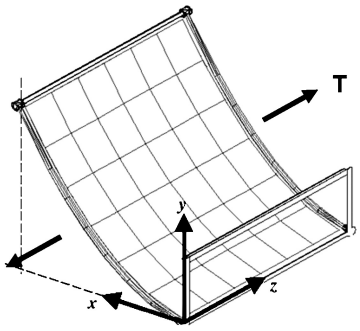

Fig. 1 Schematic representation of half-parabolic cylinder design, with tensile load (T) applied along the z direction (from Lin et al.[2]). Note that here the x axis is aligned with a line tangent to the parabola's vertex.

II. Test Article and Installation

A test plan incorporating a scale model of the precipitation radar antenna under development was submitted to the NASA Reduced Gravity Program by a group of undergraduate students at the University of Kentucky Extended Campus at Paducah. After acceptance into the program, a test fixture was designed and constructed at the Jet Propulsion Laboratory (JPL, Pasadena, California), which met

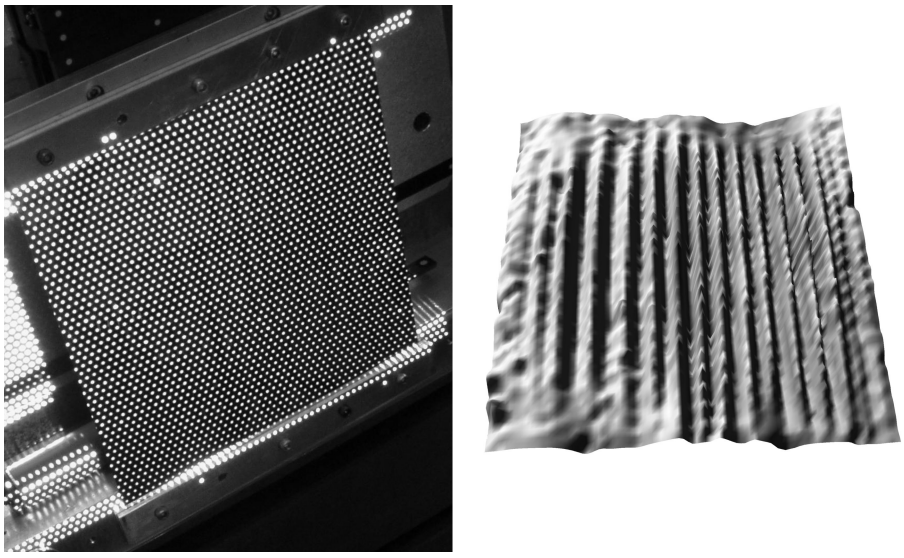

Fig. 2 Polyester membrane, 0.216×0.279 m$^2 \times 12.5e$–6 m thick, on which has been superimposed a series of projected dots used for surface targeting. The top and bottom 25.4 mm of the membrane were clamped, and a small (approximately 0.1 mm) uniaxial displacement was imposed by moving its top edge upward (normal to the edge supports). Although the vertical structural wrinkles (amplitude < 0.1 mm) developed in the membrane surface are barely visible in the photograph, they are quite obvious in the photogrammetric reconstruction of the same surface, shown on the right (from Leifer and Morgan[10]).

Fig. 3 NASA's KC-135A "Weightless Wonder" as it approaches the top of its parabolic trajectory (from NASA Reduced Gravity website).**

Fig. 4 Undergraduates performing an experiment in the 0-*g* conditions aboard the KC-135A (from NASA Reduced Gravity website).**

the weight and size restrictions imposed by the interior dimensions of the KC-135A. The fixture accommodated a truncated half-scale model of the full-size membrane, with $p_t = 0.9275$ m, $x_t = 1.27$ m, and $z_t = 1.00$ m. The test article was clamped into the fixture using two sets of cork-lined clamps that maintained the intended parabolic shape along the membrane edges normal to the z direction. One set of parabolic clamps was fixed, whereas the z position and angular orientation of the other set of clamps could be varied within a small range. This enabled a known uniaxial displacement to be applied to the edge of the membrane.

Figure 5 provides a full view of the JPL test article and fixture, shown mounted in the outer frame designed and assembled at the University of Kentucky. The exterior dimensions of the frame were designed to fit into the $1.524 \times 1.524 \times 0.914$ m^3 test volume allowed aboard the KC-135A. The cylindrical component of strain imposed on the membrane ε_z was regulated by the set of cantilevered flexors shown at the top- and bottom-left sides of the membrane test fixture. A detailed view of one of the flexors is shown in Fig. 6. Each of the flexors was fixed to one end of the variable-position membrane clamp and was mounted so that the fixed end of each flexor was located to the left of the membrane's left edge, as shown schematically in Fig. 7. This ensured that the membrane was in a state of tension in its initial configuration.

Rotation of the set screws (Fig. 8) allowed the displacement or angular rotation of the adjustable clamp to be varied, resulting in changes to the surface wrinkle configuration of the membrane. For instance, simultaneously tightening the top set screw and loosening the bottom one induced a positive counterclockwise clamp rotation about the y' axis, which allowed the imposed cylindrical component

Fig. 5 Overview of parabolic membrane, test fixture, and frame.

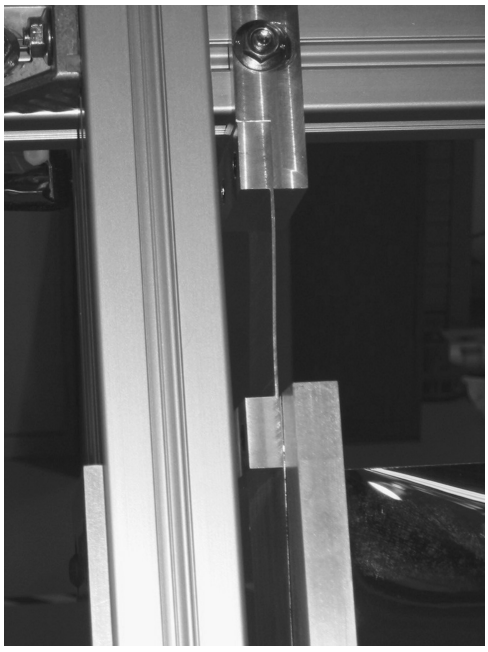

Fig. 6 Close-up view of the flexor controlling the position of the membrane clamp. Here, the flexor is the thin, flexible metal piece connecting between the extruded aluminum frame and the clamp containing the membrane that is visible in the lower-right portion of the image.

of strain $\varepsilon_z(x')$ to be varied linearly along the length of the clamp (in the x' direction). Tightening both sets of screws by the same amount uniformly increased the z position along the length of the membrane clamp by moving it to the right, which simultaneously increased the deflection of the flexors in the z direction. This effectively reduced the magnitude of the imposed cylindrical component of strain $\varepsilon_z(x')$ and hence the cylindrical component of stress $\sigma_z(x')$ generated in the membrane. After a state corresponding to a low tension was attained in the membrane by displacing the clamp sufficiently to the right, the dial gauges adjacent to the screws were set to zero. Displacements were then delivered to the membrane edge by

**Data available online at http://zerog.jsc.nasa.gov.

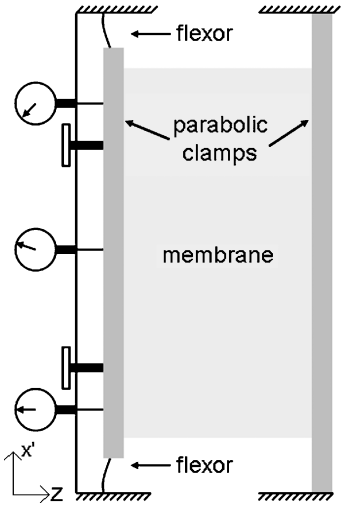

Fig. 7 Schematic representation of the membrane, tensioning flexors, set screws, and dial gauges, shown with the fixed set of clamps on the right and the moving set of clamps on the left. The dial gauges, aligned along the x' axis, were installed at intervals of 0.43 m.

Fig. 8 Photograph of dial gauge and set screw used to adjust the angle of the membrane clamp.

slightly adjusting the position and angle of the left clamp using the set screws. Positive gauge readings were obtained by loosening the set screws; this caused the flexors to pull the membrane clamp to the left. Clamp rotation about the y' axis was determined by recording the local clamp displacement using each of the three dial gauges. All wrinkles induced using this technique were reversible, as they could be eliminated by returning the set screws to their original positions, signified by a zero deflection reading on each of the dial gauges. The maximum membrane strain possible using this apparatus was obtained by completely loosening the set screws. This resulted in a force applied to the membrane edge whose magnitude was equal to the restoring force supplied by the cantilevered flexors. For intermediate set-screw positions, the z component of the stress induced in the membrane is approximated by

$$\sigma_x(x') = E\varepsilon_z(x') \tag{2}$$

where assuming $\Delta z(x')$ is the local displacement of the edge clamp, $\varepsilon_z(x')$, the cylindrical component of strain generated by the edge displacement, is

$$\varepsilon_z(x') = \Delta z(x')/z_t \tag{3}$$

Full-field deflection measurement of the membrane surface was obtained through the use of photogrammetry, a method by which three-dimensional geometry is reconstructed using a series of two-dimensional images taken from different locations around the test article. Photogrammetric techniques have been applied to the measurement of Gossamer structures by various researchers over the past few years using both fixed and projected targets.[9–14] A few of the 7000, 2–3-mm fixed targets stenciled on the membrane surface tested in this study are visible in Fig. 8; projected targets (which permit only out-of-plane displacement components to be measured) are shown on the test article depicted in Fig. 2.

Four 5.0-Megapixel "pro-sumer" grade digital cameras were installed in the membrane enclosure and used to take the images used for the photogrammetric analysis. In photogrammetry, best results are obtained when there is a 90-deg angle of separation between

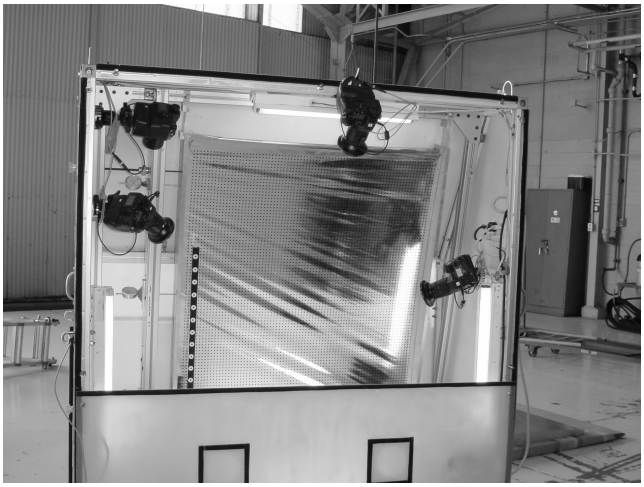

Fig. 9 Membrane enclosure showing cameras installed around its perimeter. The final arrangement used four cameras: 1) installed in enclosure front panel (removed for this picture), 2) mounted midway up right side of enclosure, 3) mounted in lower-left corner, and 4) mounted in lower-right corner.

each of the cameras used, which generally requires that the cameras be positioned at each corner of a test article. However, because of the close proximity of the cameras to the test article in this case, locations at the midright side and bottom corners of the membrane, as well as one directly in front of the membrane (mounted through the door), were chosen (Fig. 9).

Wide-angle lens extensions were used to maximize the field of view for each camera. The cameras were mounted to the enclosure using universal tripod connectors. To reduce the effect of air currents on the membrane deflection, sheet metal sides were added to the box, with access provided via a hinged front door. Reflections on the membrane from within the box were minimized by painting the interior white and enclosing the body of the cameras within white hoods. Lighting was provided by mounting fluorescent tubes on the interior of the enclosure. Images of the membrane were taken simultaneously via remote electronic camera triggers, and adjustments to the membrane clamp were made through openings on the left side of the enclosure. The fully assembled test structure, showing the adjustment openings located on the left side as well as the door-mounted camera, is visible in Fig. 4. A thick foam pad shown between the test structure and the cabin floor was used in flight to reduce the transmission of engine vibration that could have caused blurring of the test article photographs.

III. Experimental Procedure

The surface configurations of a nylon-backed Al-metallized Mylar (PET) membrane were evaluated in 0- and 1-g using the apparatus described in the preceding section. The properties of nylon-backed Mylar (PET) test membrane are as follows: the thickness t of the nylon layer is 76.2 μm, the Mylar layer is 12.7 μm, the adhesive layer is $\sim$12.7 μm, and the Al metallization is 0.1 μm; the E is 0.7 GPa; and the areal density is 0.066 kg/m^2. This particular material was chosen for evaluation because of its resistance to ripping provided by the fabric backing. Damage-resistant materials such as these are quite desirable for use in space structures that cannot be retrieved and repaired after deployment. This material was provided by JPL and was manufactured by Sheldahl (Northfield, Minnesota) in the 1970s. It was most notably used for the parasol umbrella shield deployed to shade the Skylab 1 Orbital Workshop in 1973 after problems caused by overheating were detected.[15] The nylon fabric appeared to be an orthogonal, plain, and balanced (similar structure along warp and weft directions) two-dimensional weave[16] and was of a rip-stop design, where the fabric count (number of yarns per unit length) was increased every 4 mm in both the warp and the weft directions. This produced the "checkerboard" appearance readily apparent in Fig. 10.

Table 1 Predefined gauge settings that determined the orientation of the membrane support clamp with respect to the x' axis

Setting	Bottom gauge, mm; mil	Middle gauge, mm; mil	Top gauge, mm; mil	Rotation angle, deg[a]
1	0; 0	0; 0	0; 0	0
2	3.048; 120	2.032; 80	1.016; 40	0.136
3	0.762; 30	0.381; 15	0; 0	0.051
4	1.524; 60	0.762; 30	0; 0	0.102
5	2.286; 90	1.143; 45	0; 0	0.153
6	3.048; 120	1.575; 62	0.102; 4	0.197
7	3.048; 120	1.651; 65	0.254; 10	0.186
8	3.048; 120	1.778; 70	0.508; 20	0.186
9	3.048; 120	1.905; 75	0.762; 30	0.169
10	3.048; 120	2.032; 80	1.016; 40	0.136
11	4.572; 180	3.556; 140	2.540; 100	0.136
12	3.556; 140	2.286; 90	1.016; 40	0.169
13	3.810; 150	2.413; 95	1.016; 40	0.186
14	4.191; 165	2.667; 105	1.143; 45	0.203
15	4.572; 180	2.794; 110	1.016; 40	0.237
16	4.572; 180	2.985; 117.5	1.397; 55	0.212
17	4.572; 180	3.175; 125	1.778; 70	0.186
18	4.572; 180	3.366; 132.5	2.159; 85	0.161
19	4.572; 180	3.556; 140	2.540; 100	0.136
20	3.048; 120	2.032; 80	1.016; 40	0.136
21	0; 0	0; 0	0; 0	0

[a]Indicated rotation angle for each setting (calculated using gauge readings) was clockwise.

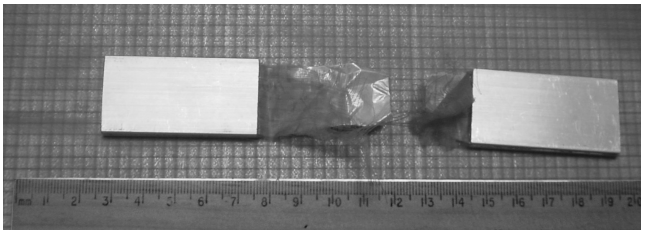

Fig. 10 Mylar-backed nylon and pull-test sample (after failure) that shows the nylon/Mylar delamination that preceded total material failure. The locations of increased fabric count along the warp, and weft directions are clearly visible. The numbers in the scale indicate units of mm × 10.

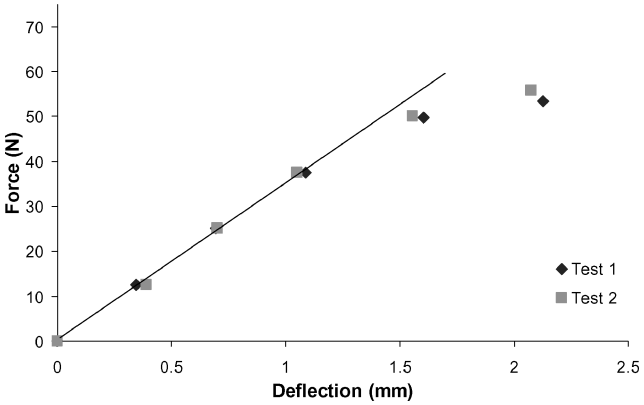

Fig. 11 Linear portion of tensile test curves obtained for the two samples of nylon-backed Mylar evaluated.

Because information pertaining to the elastic modulus of this material is no longer available, a tensile test was performed to roughly determine the material's behavior. Two 152.4×25.4 mm^2 wide strips of the nylon-backed Mylar were prepared for evaluation and oriented so that the load axis coincided with the fabric warp (Fig. 10). The outer 50.8-mm portions on each end of the membrane were sandwiched between 3.175-mm-thick strips of 50.8×25.4 mm^2 wide aluminum using contact cement. The resulting samples, which each contained a 50.8×25.4 mm^2 wide test section, were tested to failure using an Instron Universal Testing Machine at an applied displacement rate of about 0.5 mm/s. The linear-elastic portion of the force-deflection curves produced for both tests is shown together in Fig. 11. Yielding began at a deflection of slightly more than 1.0 mm for both samples, which corresponds to a yield strain of about 2%. The deflection δ for a linear material deforming elastically can be computed using

$$\delta = PL/AE \tag{4}$$

where P is the applied tensile force, L the initial length of deforming test section, and A the cross-sectional area. Using the values provided for the test-section width, length, and thickness, a linear regression calculation was performed, which yielded a value of $E = 0.7$ GPa. The correlation coefficient computed for this regression was $R^2 = 0.998$.

Using the experimental setup described in the preceding section, the structural wrinkling and gravity-induced sag of the membrane were investigated in both 0- and 1-g. The membrane was installed in its enclosure with its x' axis tilted forward by 12.4 deg with respect to the vertical direction, as shown in Fig. 9. This particular tilted orientation was chosen so that the membrane enclosure would fit into the space provided within the KC-135A cabin. Note that this installation angle determined the orientation of the gravity vector with respect to the membrane.

Two membrane test sequences were performed: a ground series at 1-g and a flight series at 0-g. After the membrane was installed in the test fixture, a single zero point was chosen by adjusting the set screws so that all visible slack was eliminated from the membrane. The dial gauges were then set to zero. This zero setting was not changed, nor was the membrane removed from the clamps, until both the ground and in-flight measurements were completed.

The standardized array of gauge settings devised for the membrane tests is shown in Table 1. A positive gauge reading in Table 1 indicates a support displacement in the negative z direction at the gauge location (indicated schematically in Fig. 7). Setting 1 provided the least amount of tension, and the gauge settings were designed so that the highest tensions were applied along the bottom of the membrane, as indicated by the higher gauge settings. Using the largest rotation angle θ along with the lowest gauge reading δ_0 corresponding to that particular angle (Table 1, setting 15), the magnitude of the displacement $\delta_{\max}$ imposed on the membrane edge can be approximated using

$$\delta_{\max} = \delta_0 + x_t \sin\theta \tag{5}$$

Assuming the projected length of the membrane $x_t = 1000$ mm, this corresponds to a value of $\delta_{\max} = 1.016 + (1000)\sin(0.237) = 5.15$ mm. For $z_t = 1000$ mm, this means that the maximum value of imposed cylindrical strain ε_z did not exceed 0.5%, a value that is well below the experimentally observed elastic limit for this material.

A surface measurement for a given membrane support condition was obtained by first rotating each set screw until the predetermined gauge readings were obtained and then triggering the cameras to create simultaneous images of the membrane from each vantage point. The gauge adjustment procedure was standardized to ensure that each time the membrane was tested it was subjected to the same loads in the same sequence. Several membrane settings (e.g., 1 and 21; 2, 10, and 20) were repeated to accommodate evaluation of measurement repeatability.

The experimental sequence was determined by the KC-135A flight schedule and allowed a complete set of ground images to be made before the flight tests performed aboard the aircraft. Before both the ground and the flight test, the membrane was set to the setting 1 point using the set screws and the dial gauges. After each edge configuration was reached, a set of images was taken by triggering the cameras simultaneously. Images were stored on 1-GByte microdrives located in each camera, which allowed up to 65 15-MByte images to be stored on each camera between downloads to an external computer hard disk drive. Although four cameras were installed in the membrane enclosure, the trigger controlling camera 4 (located on the lower-right side of the membrane) failed almost immediately after takeoff of the flight, but after completion of the 1-g ground sequence taken before takeoff. This trigger failure could not be corrected in flight; hence, the ground tests provided four images per membrane setting, whereas the flight experiments provided only three images each.

IV. Results and Discussion

Although images of the nylon-backed Mylar membrane were obtained at both 0- and 1-g for all configurations listed in Table 1, evaluation of only six sets has been performed: ground and flight images for setting 1 (the "zero" state determined shortly after the membrane was installed in the clamps) and ground and flight images for settings 3 and 5.

Because of the loss of camera 4 for the duration of the 0-g flight test, the three-dimensional contour of the entire membrane surface could not be reconstructed. Other issues, including reflections and shadows that reduced the contrast between the targets and the background in certain regions of the membrane, also caused difficulties with surface contour reconstruction, even for the ground experiments that used all four cameras. As a result, the reconstructed region of the nylon/Mylar membrane was limited to a central portion of each membrane, as indicated by the region demarcated by the plus + symbols (Fig. 12). The linear dimensions of the reconstructed area (projected into the x'–z axis) were approximately 0.37×0.5 m^2. In addition to the demarcated targets on the membrane surface, targets located on a rigid reference frame, with axes parallel to the x' and z directions, were also identified and located within each image. The targets on this frame were used to properly orient and scale the optical reconstruction of the membrane surface.

Quantitative analysis of each set of images was completed using PhotoModeler 5.0, a commercially available photogrammetry software package. (PhotoModeler is a trademark of Eos Systems Inc., Vancouver, BC, Canada.) Through iterative triangulation calculations, the software computed the three-dimensional location of each target, as well as the location of each camera. The accuracy of the three-dimensional surface reconstruction is largely dependent upon the accuracy with which targets are identified in the two-dimensional images. Generally, that resolution is limited to the ground sample distance (GSD) of the camera, which corresponds to one pixel width on the two-dimensional image of the physical test article. The cameras used here produce images that have a resolution of 2560×1920 pixels.[2] However, the close proximity of each camera to the test article means that the GSD was not constant across the images used here. This is illustrated by the image shown in Fig. 12, in which the oblique orientation of the test article makes each target in the lower-right region of the photo (GSD ~0.15 mm/pixel) appear much bigger than the targets located in the top-left region (GSD ~0.5 mm/pixel). To improve this resolution, PhotoModeler identifies each filled target in a two-dimensional image (such as ellipses or circles that extend over four or more pixels) by automatically calculating the location of its centroid. It does this by using a pixel thresholding algorithm that identifies the edge of each target and then computes the centroid of the region enclosed by each resulting target boundary. Because the calculated location of each target centroid most likely does not correspond to the center of any particular pixel, this method has been referred to as a subpixel target identification technique. Although this method has been reported to provide improvements in positioning accuracy of up to an order of magnitude over that provided by simply identifying the pixel that most closely corresponds to the center of each target,[11] the nonoptimal camera positions dictated by the test volume size, as well as their close proximity to the test article, likely limit the improvements yielded by the subpixel identification algorithms in this case. Therefore, the membrane deflections reported can be assumed accurate to at least ±0.25 mm.

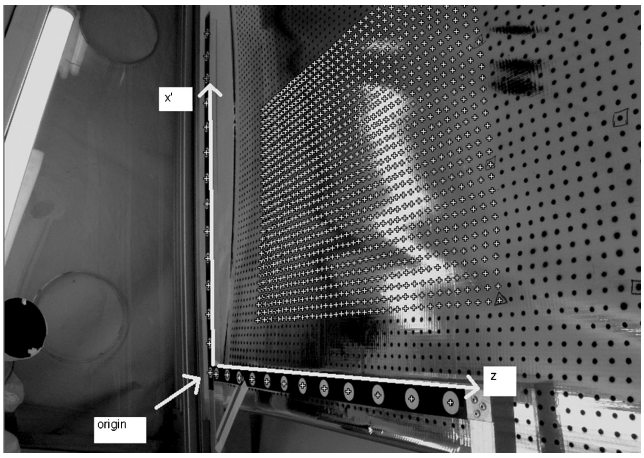

Fig. 12 View of nylon-backed Mylar membrane from camera 4. The area highlighted by the plus + symbols (approximately 0.37×0.5 m^2) was reconstructed using photogrammetry. Note the lens of camera 3, located in the bottom-left corner and the external reference frame installed around the left and bottom sides of the membrane. The dark patches located to the right side of the highlighted region indicated low-contrast areas where target identification was difficult. The x' and z directions, as well as (0,0,0) reference point located on the fixed axis, have been demarcated by arrows.

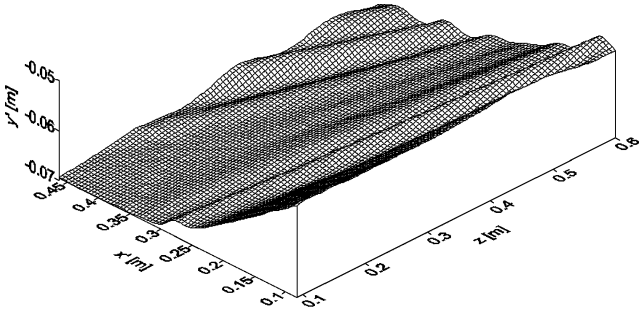

Fig. 13 Nylon/Mylar membrane surface contour for boundary setting configuration 1, flight experiment (0-g).

Each set of points on the membrane identified by the photogrammetry software was reported in three-dimensional Cartesian coordinates (x'–y'–z) and was then processed using a commercially available contouring package. This particular software used a Kriging algorithm to create a grid of regularly spaced points from each set of discrete data imported from PhotoModeler. A surface was then fit through the grids to produce the results presented next. Figures 13–18 show the reconstructed contours of the nylon/Mylar

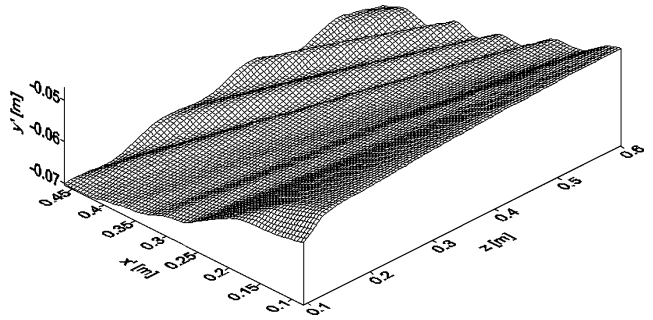

Fig. 14 Nylon/Mylar membrane surface contour for boundary setting configuration 1, ground experiment (1-*g*).

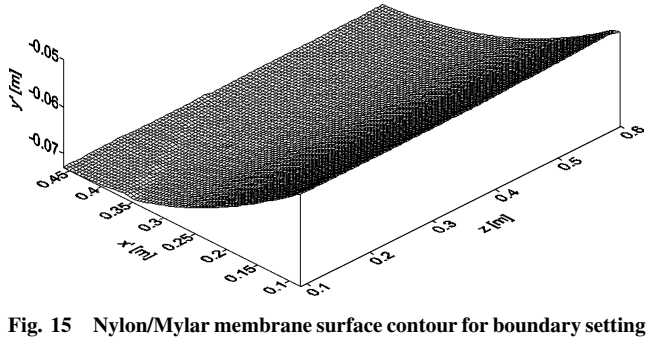

Fig. 15 Nylon/Mylar membrane surface contour for boundary setting configuration 3, flight experiment (0-*g*).

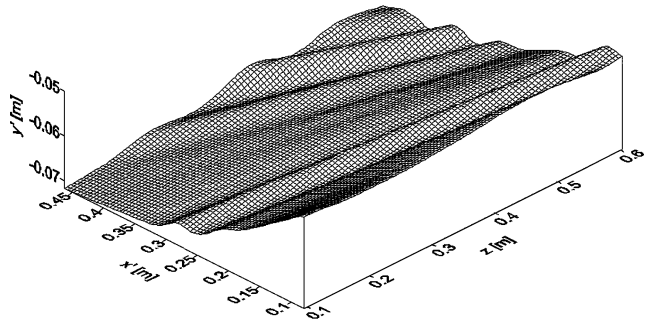

Fig. 16 Nylon/Mylar membrane surface contour for boundary setting configuration 3, ground experiment (1-*g*).

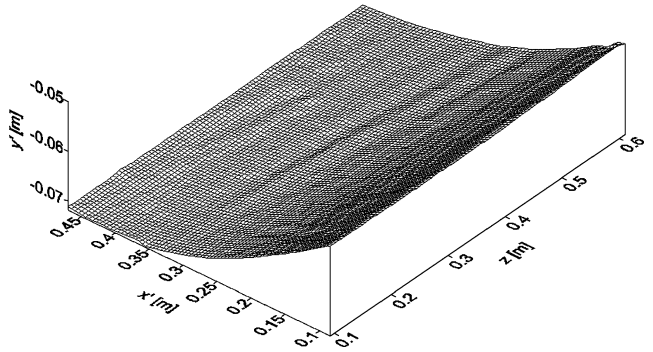

Fig. 17 Nylon/Mylar membrane surface contour for boundary setting configuration 5, flight experiment (0-*g*).

membrane at test configurations 1, 3, and 5, for both 0- and 1-*g*. The (0,0,0) point was defined at the same place on each plot and corresponded to the point located at the intersection of the two fixed reference axes indicated in Fig. 12.

Although the experimental results shown do not represent the complete set of membrane boundary configurations tested, a number of observations and generalizations can be drawn from the data presented here.

1) For a given membrane boundary configuration, the amount of surface wrinkling decreased significantly in the absence of gravity.

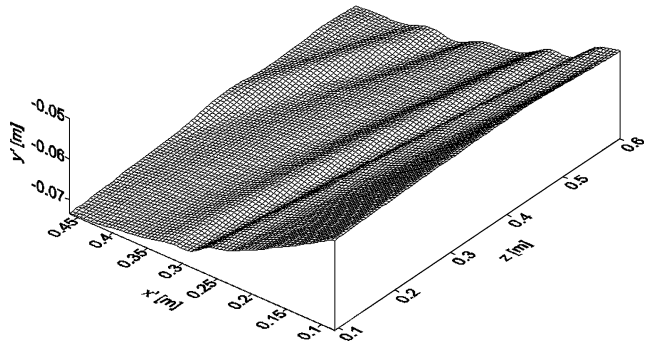

Fig. 18 Nylon/Mylar membrane surface contour for boundary setting configuration 5, ground experiment (0-*g*).

Although this effect was most dramatic for the two higher tension configurations 3 and 5 (Figs. 15 and 17), structural wrinkling also decreased in the low-tension configuration 1 (Fig. 13).

2) In all cases except for the configuration 3 flight experiment (which exhibited virtually no wrinkling), σ_1 was directed along lines extending from the bottom-right (z high, x' low) to the top-left (z low, x' high) portion of the membrane. This particular orientation of σ_1 most likely occurred in each case because of a poor choice of clamp orientation for the preset zero point, which caused the stresses to be oriented in this fashion. One possible strategy for ensuring membrane alignment and uniform loading is to observe the membrane's wrinkle pattern while it is being installed in the clamps and select a zero point that provides for horizontally oriented structural wrinkles.

3) Despite the membrane's initial misalignment at the zero set point, a virtually wrinkle-free surface was obtained in 0-*g* using border configuration 3 (Fig. 15). Although both configurations 1 and 5 (Figs. 13 and 17) possessed smoother profiles in 0-*g* than in 1-*g*, neither one of these configurations was completely wrinkle free. Based on these preliminary results, it seems likely that a border configuration that meets the rms surface accuracy levels listed in Sec. I can be found in 0-*g* regardless of any initial membrane misalignment. However, such low-wrinkle states might not be described or predicted by simple linear models or tensioning schemes. If neither an analytical nor a numerical model of high enough fidelity can be developed to determine the optimum support configuration prior to launch, one strategy for meeting rms surface accuracy requirements might be to incorporate adjustable tensioners in to the final support structure of the precipitation radar antenna. After deployment to final shape in 0-*g* (but before final release on orbit), these tensioning actuators could be adjusted to minimize structural wrinkling, thereby achieving the required surface accuracy.

V. Conclusions

The work described herein has shown that it is possible to use photogrammetry to resolve differences in membrane surface wrinkling that occur for different boundary supports and gravitational conditions. The data clearly show that deviation from the parabolic profile imposed at the clamps is more apparent in 1-*g* than in 0-*g*, and that the intended profile can likely be maintained in 0-*g* through boundary control and tensioning. Besides continued analysis of additional data from this series of experiments, photogrammetric surface data from a 0-*g* flight of a 25-μm Kapton HN membrane mounted in the same parabolic fixture have been obtained and are currently being analyzed. (Kapton is a registered trademark of the DuPont Corporation, Wilmington, Delaware.) That particular experiment concentrated on measurement repeatability, evaluated by taking multiple sets of images per boundary configuration setting. In addition, data from a series of related ground experiments, which changed the orientation of the membrane with respect to the gravity vector by rotating it about the z axis, have been obtained for the same boundary configurations evaluated in 0-*g*. These new data will likely enable correlation between the experimentally determined surface configurations and the high-fidelity computational models currently under development.

Acknowledgments

The authors thank the Kentucky Space Grant Consortium, the University of Kentucky Vice President for Research, the NASA Faculty Fellowship Program, and the University of Kentucky Extended Campus Program at Paducah for financial assistance; and Sally Smith-Clemens and William Carp of Olympus USA for donating their time and one of the cameras used for this project. Thanks also to the Paducah Weightless Wildcats (PaWWs) ground-support team in Houston (Kara Adair, Josh Medley, Jason Perry, and Christian Musselman) and PaWWs flight crew members Justin Hastie and Ben Morgan. Finally, thanks to Jon Black of NASA Langley Research Center, Joe Blandino of James Madison University, and Carl Knoll of ILC-Dover for their technical advice; and to Fadi Kamal Abu-Farha, Ph.D. Student in the University of Kentucky Department of Mechanical Engineering, who performed the tensile tests on the nylon-Mylar samples. Access to the KC-135A was provided through the NASA Reduced Gravity Student Flight Opportunities Program.

References

[1]Im, E., Durden, S. L., Kakar, R. K., Kummerow, C. D., and Smith, E. A., "The Next Generation of Spaceborne Rain Radars: Science Rationales and Technology Status," *Proceedings of the Third Symposium on Microwave Remote Sensing of the Atmosphere and Environment*, Society of Photo-Optical Instrumentation Engineers (International Society for Optical Engineering), Bellingham, WA, 2002.

[2]Lin, J. K., Sapna, G. H., III, Scarborough, S. E., and Lopez, B. C., "Advanced Precipitation Radar Antenna Singly Curved Parabolic Antenna Reflector Development," AIAA Paper 2003-1651, April 2003.

[3]Lopez, B. C., Lih, S-S., Leifer, J., and Guzman, G., "Study of Ripple Formation in Unidirectionally-Tensioned Membranes," AIAA Paper 2004-1737, April 2004.

[4]Blandino, J. R., Johnston, J. D., and Dharamsi, U. K., "Corner Wrinkling of a Square Membrane Due to Symmetric Mechanical Loads," *Journal of Spacecraft and Rockets*, Vol. 39, No. 5, 2002, pp. 717–724.

[5]Wong, Y. W., and Pellegrino, S., "Computation of Wrinkle Amplitudes in Thin Membranes," AIAA Paper 2002-1369, April 2002.

[6]Wong, Y. W., and Pellegrino, S., "Amplitude of Wrinkles in Thin Membranes," *New Approaches to Structural Mechanics, Shells and Biological Structures*, edited by H. Drew and S. Pellegrino, Kluwer Academic, Dordrecht, The Netherlands, 2002.

[7]Jenkins, C. H., Haugen, F., and Spicher, W. H., "Experimental Measurement of Wrinkling in Membranes Undergoing Planar Deformation," *Experimental Mechanics*, Vol. 38, No. 2, 1998, pp. 147–152.

[8]Leifer, J., and Belvin, W. K., "Prediction of Wrinkle Amplitudes in Thin Film Membranes via Finite Element Modeling," AIAA Paper 2003-1983, April 2003.

[9]Black, J. T., Leifer, J., DeMoss, J. A., Walker, E. N., and Belvin, W. K., and S. W., "Experimental and Numerical Correlation of Gravity Sag in Solar Sail Quality Membranes," AIAA Paper 2004-1579, April 2004.

[10]Leifer, J., and Morgan, B. G., "Structural Wrinkling of Thin Gossamer Films Under Edge Shear," *Journal of Experimental Mechanics* (submitted for publication).

[11]Pappa, R. S., Giersch, L. R., and Quagliaroli, J. M., "Photogrammetry of a 5 m Inflatable Space Antenna with Consumer Digital Cameras," NASA TM-2000-210627, Dec. 2000.

[12]Pappa, R. S., Jones, T., Black, J. T., Walford, A., Robson, S., and Shortis, M., "Photogrammetry Methodology Development for Gossamer Spacecraft Structures," AIAA Paper 2002-1375, April 2002.

[13]Leifer, J., Black, J., Belvin, W. K., and Behun, V., "Design and Evaluation of Shear Compliant Borders for Thin Film Membrane Structures," AIAA Paper 2003-1984, April 2003.

[14]Pappa, R. S., Black, J. T., Blandino, J. R., Jones, T. W., Danehy, P. M., and Dorrington, A. A., "Dot-Projection Photogrammetry and Videogrammetry of Gossamer Space Structures," *Journal of Spacecraft and Rockets*, Vol. 40, No. 6, 2003, pp. 858–867.

[15]"Parasol" Sunshade for Skylab 1, NASA Photo ID: S73-2640123, May 1973, Spaceref Image Database, Reston, VA, URL: http://gallery.spaceref.com/us-spaceflight/SL2/10076085.html [cited 27 Dec. 2004].

[16]Naik, N. K., *Woven Fabric Composites*, Technomic, Lancaster, PA, 1994, pp. 9–11.

G. Agnes
Associate Editor